Optimizing of gas-shielded metal arc welding parameters for 10.5-12.5% chromium steel using 308L electrodes

A.M. Maleka[1,2], V.J. Matjeke[1,2], and J.W. van der Merwe[2]

Affiliation:
[1]Transnet Engineering, Kilnerpark, South Africa.
[2]School of Chemical and Metallurgical Engineering, University of the Witwatersrand, Johannesburg, South Africa.

Correspondence to:
A.M. Maleka

Email:
Audrey.Maleka@transnet.net

Dates:
Received: 28 Feb. 2022
Revised: 18 Aug. 2022
Accepted: 30 Mar. 2023
Published: April 2023

How to cite:
Maleka, A.M., Matjeke, V.J. and van der Merwe, J.W. 2023 Optimizing of gas-shielded metal arc welding paramenters for 10.5-12.5% chromium steel using 308L electrodes. Journal of the Southern African Institute of Mining and Metallurgy, vol. 123, no. 4. pp. 157-164

DOI ID:
http://dx.doi.org/10.17159/2411-9717/2037/2023

ORCID:
A.M. Maleka
http://orcid.org/0009-0004-3939-8439

Synopsis

The 10.5–12.5% chromium, titanium-stabilized ferritic stainless steel (FSS) plates used to fabricate coal line jumbo wagons is susceptible to undesirable chromium depletion during welding with 309L electrodes. In this work, non-stabilized FSS plates were welded using 308L welding electrodes. The objective was to weld non-stabilized FSSs using gas-shielded metal arc welding without causing sensitization. The welding process was optimized by lowering the heat input. Sensitization was assessed by rigorous etching techniques and anodic polarization scans. In addition, the welds were subjected to tensile testing, and their fracture surfaces were examined for intergranular cracking. Non-stabilized FSS plates were successfully welded using gas metal arc welding.

Keywords

Titanium-stabilized ferritic stainless steel, welding parameters, 308L welding electrode, gas metal arc welding, heat input.

Introduction

Titanium-stabilized ferritic stainless steels (FSSs) are widely used for structural and railway wagon applications due to their excellent corrosion and wear resistance (van Warmelo, Nolan, and Norrish, 2007). Yet many railway operators use coal wagons fabricated with mild steel due to its affordability. Mild steel readily corrodes in an environment that contains sulphur dioxide (Allen, Ball, and Protheroe, 1982; Morcillo *et al.*, 2013; Taban, Kaluc, and Dhooge, 2009; Zhang *et al.*, 2014). Titanium-stabilized FSSs are a good substitute for regular austenitic and mild steels due to their superior mechanical properties and corrosion resistance, respectively (Mursalo, Tullmint, and Robinson-, 1988; Rossi, 2010; Shojaati and Beidokhti, 2017). Furthermore, coal wagons built from titanium-stabilized FSS have lower life-cycle costs than wagons fabricated with mild steel and austenitic stainless steel (Allen, Ball, and Protheroe,1982). One of the biggest cost drivers for manufacturing railway vehicles with FSSs is the welding operation and consumables. Since 1985, railway wagons have been successfully welded with gas metal arc welding (GMAW) using titanium-stabilized FSS and 309L welding electrodes (van Warmelo, Nolan and Norrish., 2007).

Coal wagons in South Africa and Australia are currently built using titanium-stabilized FSS plates with a low carbon content, 10.5–12.5% chromium, and a maximum of 0.6% titanium (van Warmelo, Nolan, and Norrish, 2007). Titanium-stabilized FSS and the non-stabilized FSSs are produced according to EN 1.4003 classification, with the only difference being the amount of titanium (du Toit and Naudé, 2011). Using non-stabilized FSSs in the railway industry was unsuccessful due to sensitization. The function of titanium in this stainless steel is to form titanium carbides during welding to avoid chromium depletion on the grain boundaries by lowering the carbon concentration, since titanium has a higher affinity for carbon than does chromium (Sundqvist *et al.*, 2018). This reduces the possible precipitation of chromium carbides on the grain boundaries (Keskitalo *et al.*, 2015). Chromium depletion (sensitization) often results in the loss of corrosion resistance within the heat-affected zone (HAZ) along the grain boundaries (Dahmen, Rajendran, and Lindner, 2015). The non-stabilized stainless steel does not contain titanium; therefore it is more prone to sensitization during welding (Moslemi *et al.*, 2015). Laser welding of non-stabilized grade is successful due to the arc efficiency and the ability to produce a functional weld with a lower heat input (Dahmen, Rajendran, and Lindner, 2015; Pekkarinen and Kujanpää, 2010; Sundqvist *et al.*, 2018).

Generally, many stainless steels have good corrosion resistance and mechanical properties; however, precautions to avoid sensitization must be taken during welding (Sundqvist *et al.*, 2018). The EN 1.4003 grade has good formability and is cheaper than the austenitic stainless steel grades (Keskitalo *et al.*, 2015). The 308L welding electrode was selected over other welding consumables due to its distinct properties and cost efficiency (Allen, Ball, and Protheroe, 1982). The cost of 309L and 308L welding elctrodes is 17.5

and 13.9 US dollars per kg, respectively. Both the 308L and 309L welding consumables produce an austenitic microstructure. 308L welding wire and non-stabilized FSS plates have not been used to manufacture rail wagons.

GMAW generates heat from the arc between the welding electrode and the substrate with an externally supplied shielding gas (Ghosh *et al.*, 2018). This study investigated the welding properties of non-stabilized FSS (EN 1.4003) using the 308L welding electrode with GMAW. Du Toit and Naudé (2011) investigated the role of heat input on EN 1.4003 sensitization using gas tungsten arc welding. Their results showed that a low heat input may retard sensitization in non-stabilized FSS. In the current study, the welding parameters were optimized to achieve the arc efficiency that can produce quality joints in non-stabilized FSS using 308L welding electrodes, without causing sensitization during welding.

Sensitization due to continuous cooling after welding at low heat input occurs in the coarse-grained region adjacent to the fusion line in material where the HAZ is predominately ferritic (Amuda, 2011). It occurs when low heat input during welding leads to very fast cooling rates at the early stage of the weld thermal cycle. This rapid cooling can restrict or prevent austenitic nucleation as the HAZ cools through the dual phase (ά+γ) field, resulting in almost fully ferritic microstructures (Amuda, 2011).

Optimizing the welding parameters regulates the heat input sufficiently to produce an acceptable weld without compromising the joint quality. This paper presents the mechanical and metallurgical properties of the welded non-stabilized FSS plates without substantial dilution and chromium depletion on the HAZ. Furthermore, this study explored the susceptibility of the 1.4003/308L joints to galvanic corrosion.

Experimental procedure

Non-stabilized FSS plates supplied in the rolled and annealed condition and 308L welding electrodes were used for welding experiments. A 4 mm square butt joint with a 2 mm gap was welded using alternating current GMAW with a 1 mm diameter solid filler metal acting as an electrode. Figure 1 shows the plates before and after welding. The edges were cleaned with acetone to remove potential contaminants. The molten weld pool was protected using argon shielding gas at a flow rate of 18 L/min. A single run was deposited to join the square butt weld. The welding parameters are shown in Table I. Heat inputs of 0.45 and 0.54 kJ/mm were used to produce the respective welds.

Macroscopic examination

The welded plates were sectioned and prepared for macroscopic examination, which entailed cutting, grinding and polishing the weld transverse section, followed by etching with ammonia persulphate. The weld assessment was undertaken using a stereoscope equipped with OLYMPUS Stream essential analysis software to evaluate the weld joint quality and to measure the deposition area.

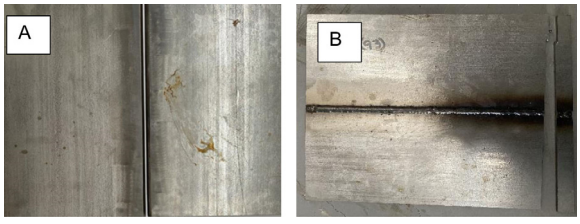

Figure 1—Non-stabilized FSS plates prior to welding (A) and after welding (B)

Chemical analysis

The chemical analysis of the parent metal was performed using a Bruker Q4 TASMAN optical emission spectrometer. The parent metal was ground to prepare it for chemical analysis. Furthermore, chemical analysis of the weld and weld joint, *i.e.*, HAZ and weld, was conducted using a Carl Zeiss scanning electron microscope equipped with an Oxford energy-dispersive spectrometer (EDS) for the map and line scan method, respectively. The samples were polished to a 1 µm surface finish before EDS analysis. The accelerated voltage was 20 kV and the exposure time was 45 seconds. The EDS point method aimed to determine the chemical composition (without carbon) of the weld, while the line scan was used to detect chromium depletion.

Microscopic examination

Transverse sections from the butt-welded joints were prepared for metallographic examination. The samples were sectioned, mounted, ground and polished to surface finish. The microstructures of the weld, parent metal, and HAZ of the welded samples were prepared for examination by grinding and polishing followed by etching with Vilella's reagent (1 g picric acid, 100 ml ethanol, and 5 ml HCl). The etched samples were examined using optical and scanning electron microscopy to detect possible cracking and weld decay. The Olympus optical microscope is equipped with Stream essential analysis software to quantify the phases of the microstructures.

Mechanical testing

The as-polished samples were tested for hardness using a DuraScan micro-Vickers hardness tester. The hardness profile measurements were taken at intervals of 0.5 mm, with a load and dwelling time of 5 kg-f and 10 seconds, respectively. The welded samples, two per welding parameter and a validation sample, were tested for tensile properties.

Table I

Weld design and welding variables

Weld	Current (A)	Voltage (V)	Heat input (kJ/mm)	Travelling speed (mm/min)
A	165-173	19-19.6	0.45	351
B	130-140	24-26	0.54	329

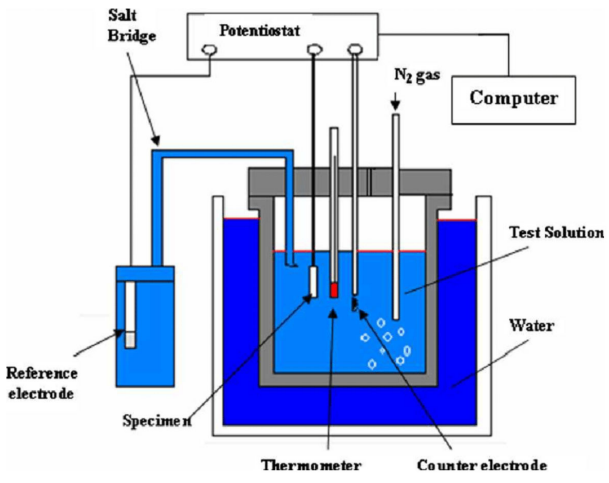

Figure 2—Schematic view of the electrochemical corrosion test set-up (Nihal, 2017)

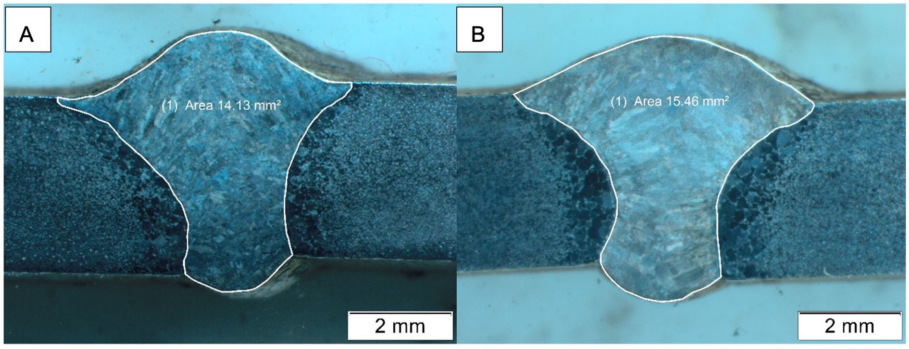

Figure 3—Weld deposition area of samples welded with (A) 0.45 kJ/mm and (B) 0.54 kJ/mm heat input

Strauss test

The polished samples were also immersed in a mixture of 3 ml sulphuric acid and 60 g copper sulphate in 100 ml of distilled water for 72 hours at boiling temperatures for intergranular corrosion testing. An Allihn condenser was used for the Strauss test experiment. This test was done in accordance with ASTM A262 practise E standard to expose the sensitized area to aggravated corrosion.

Corrosion tests

The steel welded joint was exposed to a solution of 3.5% sodium chloride and the corrosion characteristics were determined by first considering the open circuit potential for a short period. The electrochemical potential was then scanned from an active potential to a more noble potential than the corrosion potential. A Metrohm Autolab 302 potentiostat with a silver reference electrode and a carbon counter-electrode was used to perform the test. The scan rate was 0.1 mV/s. These characteristics were used to determine the corrosion rate of the steel when exposed to the environment as well as its electrochemical potential. Figure 2 shows the set-up for electrochemical corrosion test.

In addition, the galvanic current was determined between the weld metal and the non-stabilized FSS substrate under open circuit potentials by connecting the weld metal to the working electrode and the substrate to the counter-electrode. This was done according to the ISO 3651-2 method A standard.

Results and discussion

Visual examination

The welded plates revealed full penetration of the weld with no defect. Figure 3 shows macroscopic samples of the plates welded using 0.45 and 0.54 kJ/mm heat inputs. More weld deposition was observed on a macroscopicscale using a heat input of 0.54 kJ/mm.

Chemical composition and analyses

FSS containing 10.5–12.5% chromium is most likely to experience sensitization (chromium content below the required level) on the grain boundaries. The chemical compositions of the parent metal and the weld are reported in Table II. The chemical composition of the parent metal and the weld were typical of FSS and austenitic stainless steel, respectively. Composition of the weld is reported without carbon due to the inability of EDS to determine carbon.

Table II

Chemical analysis of the base metal and welding electrodes (wt%)

Material	C	Cr	Mn	Si	Mo	Ni	Cu	S	P	O	Cl	Co
Plates	0.009 ± 0.001	11.41 ± 0.06	0.86 ± 0.004	0.76 ± 0.008	0.005 ± 0.001	0.74 ± 0.017	0.14 ± 0.001	0.001 ± 0	0.02 ± 0	-	-	-
308L electrode	-	18.3 ± 1.190	1.4 ± 0.13	0.5 ± 0.001	-	8.1 ± 0.30	0.04 ± 0.001	-	-	4.0 ± 0.10	1.7 ± 0.180	0.4 ± 0.005

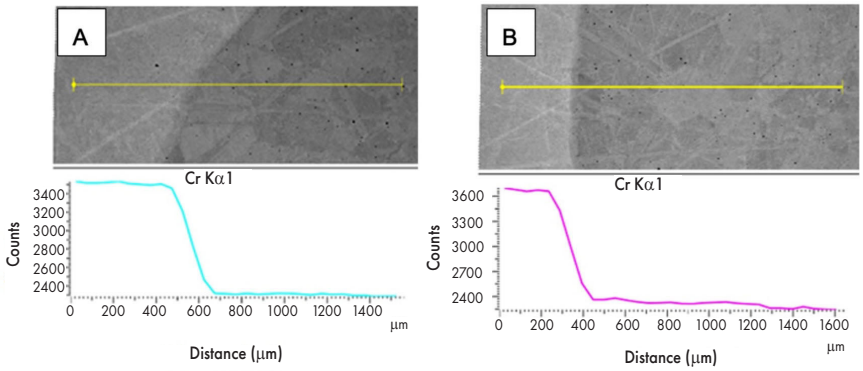

Figure 4—EDS micrographs and line scan (counts per second) for samples welded with (A) 0.45 kJ/mm and (B) 0.54 kJ/mm heat input

The chromium line scan counts per second are shown in Figure 4. No sample showed any sign of chromium depletion, therefore no sensitization occurred during welding.

Microscopic examination

Non-stabilized FSSs are generally prone to sensitization during welding. The microstructures of the parent metal and weld were used to evaluate the possible presence of sensitization (Figure 5a). The parent metal microstructure was confirmed to be ferritic.

The microstructures revealed complete fusion between the parent metal and the weld. The weld microstructures showed a needle-like lamellar austenitic texture (Figure 5b). The higher heat input corresponded with an increase in HAZ width (Figure 6).The HAZ distance measurements are shown in Table III. The general microstructures of the HAZ were found to consist of coarser ferrite grains with martensite embedded on the grain boundaries.

The formation of martensite in the HAZ is due to the temperature increase introduced by the weld pool followed by rapid cooling. Although martensite can introduce metallurgical notches, for wagon wear plates, the harder phase promotes wear resistance. Martensite was predominately observed on microstructures welded using 0.54 kJ/mm heat input. Figure 7 shows the 0.45 and 0.54 kJ/mm phase analyses. The quantitative analysis of martensite on the 308L at a heat input of 0.45 and 0.54 kJ/mm is presented in Table III.

Sensitization in FSSs is generally difficult to examine by etching and evaluation under the optical microscope. Ten per cent oxalic acid has been favoured by some researchers for both FSSs and austenitic stainless steel. In our other work, we found that Vilella's reagent (1 g picric acid,100 ml ethanol, and 5 ml HCl) revealed FSS microstructures in more detail than 10% oxalic acid. No sensitization was detected with either Vilella or oxalic reagent (Figure 8). The Strauss test was used to eliminate any doubt about the absence of sensitization. Figure 9 shows the secondary backscattered images of samples that were subjected to the Strauss test. Although details of the grain boundaries are visible, there was no sign of a ditch or dual.

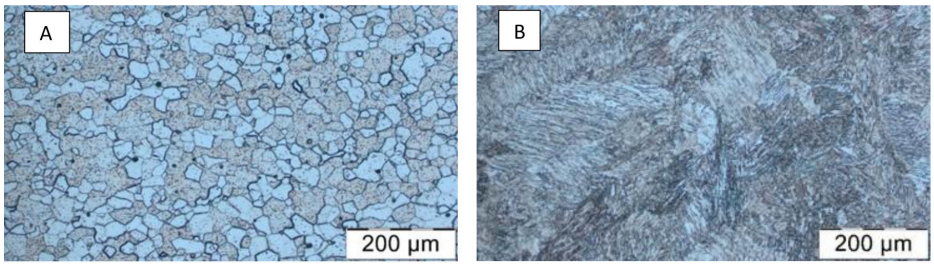

Figure 5—Weld microstructures of (A) parent metal and (B) 308L welding wire

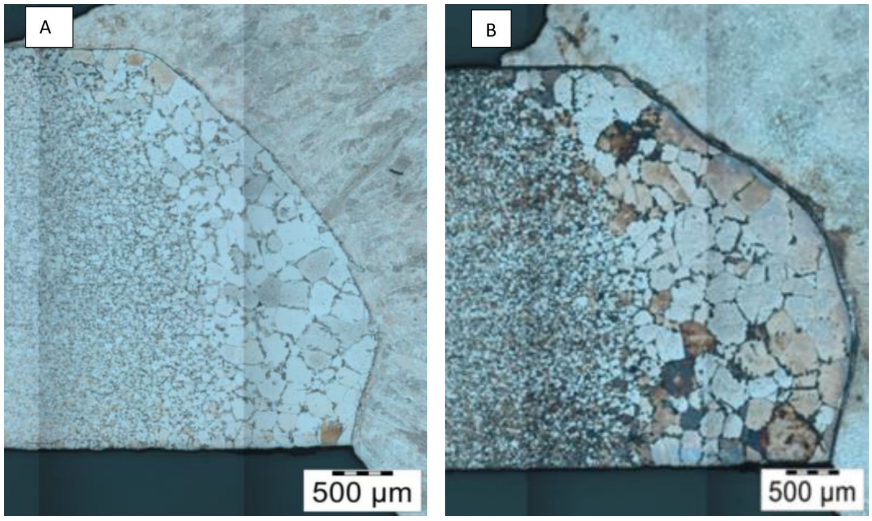

Figure 6—Stitched samples welded with (A) 0.45 kJ/mm and (B) 0.54 kJ/mm heat input

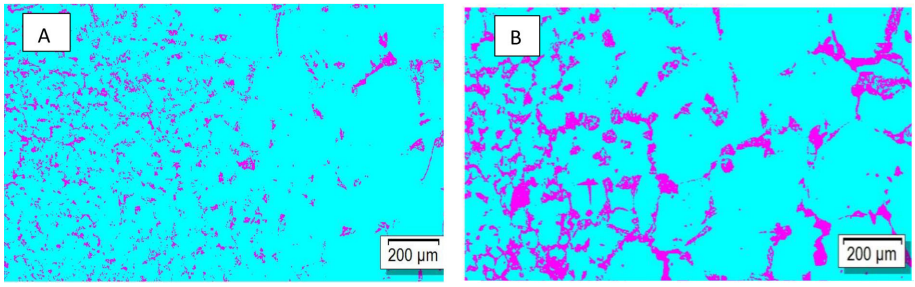

Figure 7—Phase analysis of sample welded with (A) 0.45 kJ/mm (B) 0.54 kJ/mm heat input. Pink and blue colours indicate martensite and ferrite, respectively

Table III

Measurements of heat-affected zone (HAZ) of the welded plates and martensite content

Weld sample	HAZ (µm)	Martensite (%)
0.45 kJ/mm heat input	2032	4.6
0.54 kJ/mm heat input	2243	10.95

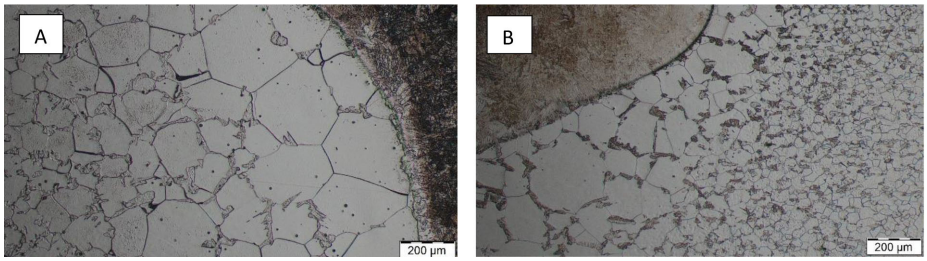

Figure 8—Samples welded with (A) 0.45 kJ/mm and (B) 0.54 kJ/mm heat input, both etched with Vilella's reagent

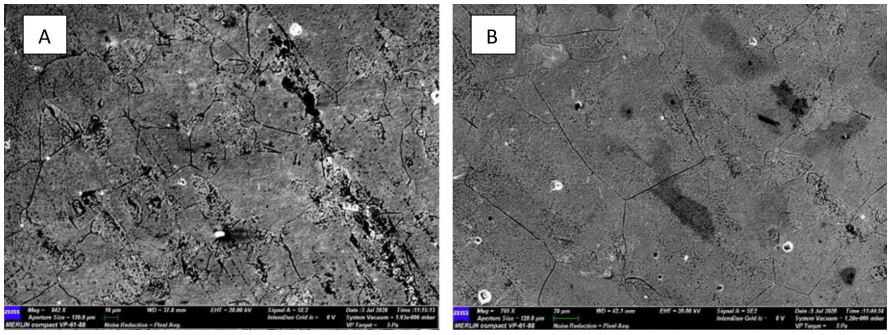

Figure 9—Secondary detector images after Strauss test of sample welded with (A) 0.45 kJ/mm and (B) 0.54 kJ/mm heat input

Mechanical properties

The weld strength and integrity were further investigated by tensile testing and fracture surface examination. The samples were machined to dimensions of 12.5 mm in width and 50 mm gauge length following the ASTM E8 machining standard. An MTS Criterion® model 45 equipped with an MTS video extensometer was used to test the samples in accordance with the SANS 6892-1:2010 standard testing method. All the tensile pieces failed on the parent metal. The tensile test results are summarized in Table IV. The fracture surfaces revealed a ductile fracture mode (Figure 10). The tensile properties of the samples welded with 0.45 and 0.54 kJ/mm heat inputs were comparable.

Table IV

Tensile properties of the ferritic stainless steel plates welded at 0.45 kJ/mm and 0.5 kJ/mm heat inputs

Mechanical properties	0.4 kJ/mm heat input	0.5 kJ/mm heat input
Yield strength (MPa)	293 ± 9	292 ± 5
Ultimate tensile strength (MPa)	429 ± 3	441 ± 10
% elongation	16 ± 2	19 ± 1

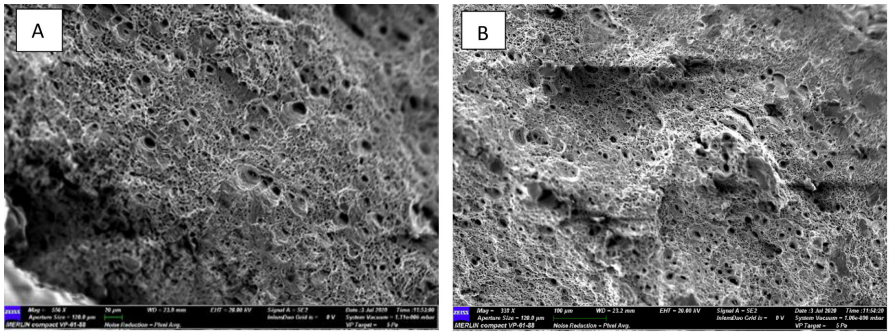

Figure 10—Fracture surfaces of the tensile test sample welded with (A) 0.45 kJ/mm and (B) 0.54 kJ/mm heat input (secondary electron images)

The hardnesses of the parent metal, HAZ, and weld were determined. The transverse hardness test profile across the weld is shown in Figure 11. The weld metal had a higher hardness than the parent metal (Table V).

Corrosion results

The potentiodynamic scans of the substrate and two weld metals after exposure to a 3.5% sodium chloride solution at 40°C are shown in Figure 12. The corrosion potentials of the weld metals and the substrate are close, indicating that the galvanic effects will be small.

The effect of the galvanic action was investigated by recording the galvanic current between the weld metal (anode) and the substrate (cathode) in the 3.5% sodium chloride solution at 40°C (Figure 13). The results are consistent with the polarization characteristics, indicating that the 308L weld metal is slightly more noble than the substrate, inducing a more negative current. All samples revealed that the complete fusion between the parent metal and the weld was more noble than the substrate, inducing a more negative current. However, the 309L weld metal starts at a negative current and then increases to become positive.

We have shown that GMAW can produce a weld without causing sensitization. This was achieved because of the rapid cooling associated with low heat input. The rapid cooling process is further confirmed by the formation of martensite. For other applications, the presence of martensite may be undesirable; however, for wagon wear plates, this phase is beneficial because of the improved hardness. Sensitization assessments were conducted using exhaustive etching techniques, microstructural analysis, and the electrochemical potentio-kinetic reactivation technique. The tensile test fracture samples did not show any intergranular cracking.

The wider HAZ and larger grain sizes are attributed to the higher heat input. However, the effect of these notches is less than that introduced by titanium carbides. Dahmen, Rajendran, and Lindner (2015) found no sensitization in grain boundarues layered with martensite. It has been observed that the percentage martensite increases with an increase in heat input due to the wider HAZ.

Table V

Average hardness values for the parent metal, heat-affected zone (HAZ), and the weld

Average hardness (Hv 0.5)	0.45 kJ/mm heat input	0.54 kJ/mm heat input
Parent metal	163 ± 3.13	161 ± 3.13
HAZ	192 ± 3.13	198 ± 3.13
Weld	215 ± 3.13	207 ± 3.13

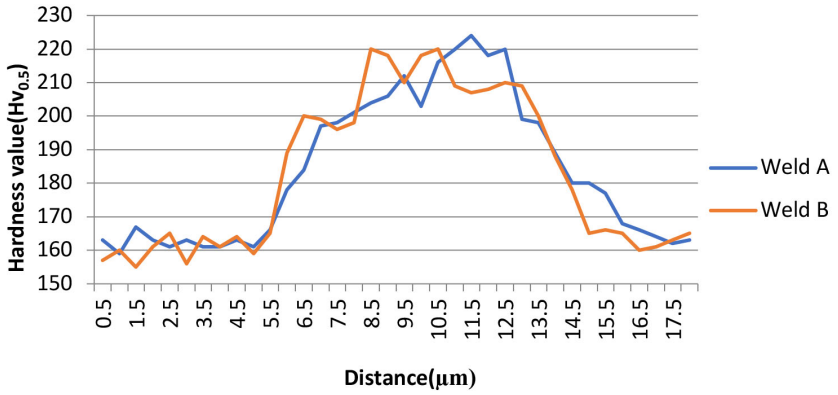

Figure 11—Microhardness profiles across the welds

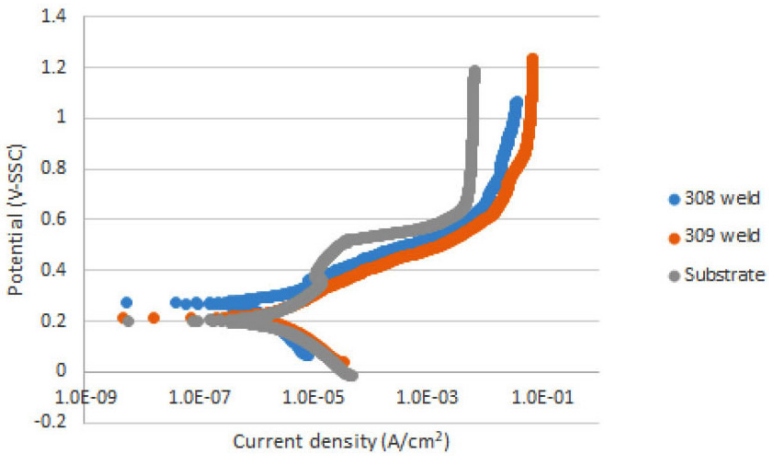

Figure 12—Potentiodynamic curves of EN 1.4003 FSS (substrate) and the 308L and 309L weld metals exposed to a 3.% NaCl solution at 40°C

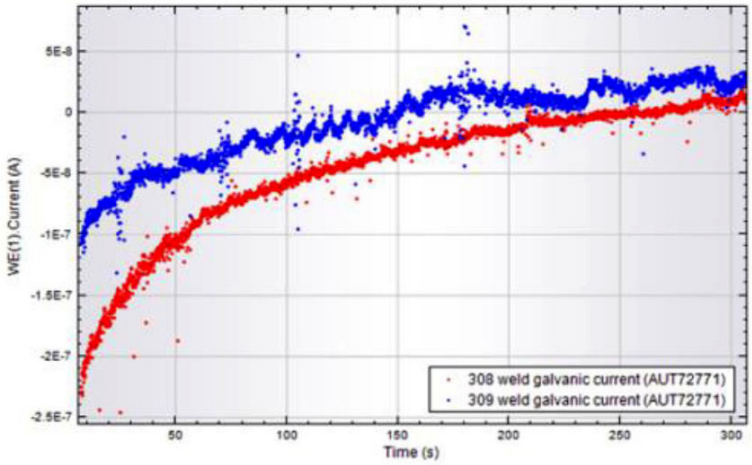

Figure 13—Galvanic current between the weld metal and substrate (EN 1.4003) in 3.5% sodium chloride at 40°C

Conclusion

This study proves that FSSs can be welded using GMAW without causing sensitization. This achievement benefits productivity because GMAW has higher arc efficiency and deposition rates. The successful welding of non-stabilized FSS and 308L electrodes is a breakthrough in the advancement of cost-effective production. Based on the tests conducted and results obtained, both 0.45 and 0.54 kJ/mm heat inputs allowed the production of full penetration and good fusion welds with no sensitization observed in any of the samples.

References

Allen, C., Ball, A., and Protheroe, B.E. 1982. The abrasive-corrosive wear of stainless steels. *Wear*, vol 74, no. 2. pp. 287–305. https://doi.org/10.1016/0043-1648(81)90169-1

Amuda, M.O.H. 2011. An overview of sensitization dynamics in ferritic stainless steel welds. *International Journal of Corrosion*, vol. 2011. Article 305793. http://dx.doi.org/10.1155/2011/305793

Dahmen, M., Rajendran, D.K., and Lindner, S. 2015. Sensitization of laser-beam welded martensitic stainless steels. *Physics Procedia*, vol. 78. pp. 240–246. https://doi.org/10.1016/j.phpro.2015.11.034

Du Toit, M. and Naudé, J. 2011. The influence of stabilization with titanium on the heat-affected zone sensitization of 11 to 12% chromium ferritic stainless steels under low heat input welding conditions. *Welding in the World*, vol. 55, pp. 38–47.

Ghosh, N., Pal, P.K., Nandi, G., and Rudrapati, R. 2018. Parametric optimization of gas metal arc welding process by PCA based Taguchi method on austenitic stainless steel. *Materials Today: Proceedings*, vol. 5, no. 1. pp. 1620–1625. https://doi.org/10.1016/j.matpr.2017.11.255

Keskitalo, M., Sundqvist, J., Mäntyjärvi, K., Powell, J., and Kaplan, A.F.H. 2015. The influence of shielding gas and heat input on the mechanical properties of laser welds in ferritic stainless steel. *Physics Procedia*, vol. 78. pp. 222–229. https://doi.org/10.1016/j.phpro.2015.11.032

Morcillo, M., Chico, B., Díaz, I., Cano, H., and de la Fuente, D. 2013. Atmospheric corrosion data of weathering steels. A review. *Corrosion Science*, vol. 77. pp. 6–24. https://doi.org/10.1016/j.corsci.2013.08.021

Moslemi, N., Redzuan, N., Ahmad, N., and Hor, T.N. 2015. Effect of current on characteristic for 316 stainless steel welded joint including microstructure and mechanical properties. *Procedia CIRP*, vol. 26. pp. 560–564. https://doi.org/10.1016/j.procir.2015.01.010

Mursalo, N., Tullmint, M., and Robinson, F.P.A. 1988. The corrosion behaviour of mild steel, 3CR12, and AISI type 316L in synthetic minewaters. *Journal of the South African Institute of Mining and Metallurgy*, vol. 88, no. 8. pp. 249–256.

Pekkarinen, J. and Kujanpää, V. 2010. The effects of laser welding parameters on the microstructure of ferritic and duplex stainless steels welds. *Physics Procedia*, vol. 5. pp. 517–523. https://doi.org/10.1016/j.phpro.2010.08.175

Rossi, B. 2010. Mechanical behavior of ferritic grade 3Cr12 stainless steel—Part 1 : Experimental investigations. *Thin-Walled Structures*, vol. 48, no. 7. pp. 553–560. https://doi.org/10.1016/j.tws.2010.02.008

Shojaati, M. and Beidokhti, B. 2017. Characterization of AISI 304/AISI 409 stainless steel joints using different filler materials. *Construction and Building Materials*, vol. 147. pp. 608–615. https://doi.org/10.1016/j.conbuildmat.2017.04.185

Sundqvist, J., Manninen, T., Heikkinen, H.-P., Anttila, S., and Kaplan, A.F.H. 2018. Laser surface hardening of 11% Cr ferritic stainless steel and its sensitisation behaviour. *Surface and Coatings Technology*, vol. 344. pp. 673–679. https://doi.org/10.1016/j.surfcoat.2018.04.002

Taban, E., Kaluc, E., and Dhooge, A. 2009. Hybrid (plasma + gas tungsten arc) weldability of modified 12% Cr ferritic stainless steel. *Materials & Design*, vol. 30, no. 10. pp. 4236–4242. https://doi.org/10.1016/j.matdes.2009.04.031

Van Warmelo, M., Nolan, D., and Norrish, J. 2007. Mitigation of sensitisation effects in unstabilised 12%Cr ferritic stainless steel welds. *Materials Science and Engineering: A*, vol. 464, no. 1–2. pp. 157–169. https://doi.org/10.1016/j.msea.2007.02.113

Zhang., X, Yang, S., Zhang, W., Guo, H., and He, X. 2014. Influence of outer rust layers on corrosion of carbon steel and weathering steel during wet–dry cycles. *Corrosion Science*, vol. 82. pp. 165–172. https://doi.org/10.1016/j.corsci.2014.01.016 ◆